



# Optical and Geometrical Properties of Cirrus Clouds in Amazonia Derived From 1-year of Ground-based Lidar Measurements

Diego A. Gouveia<sup>1</sup>, Boris Barja<sup>1,2</sup>, Henrique M. J. Barbosa<sup>1</sup>, Theotônio Pauliquevis<sup>3</sup>, and Paulo Artaxo<sup>1</sup>.

<sup>1</sup>Applied Physics Department. Institute of Physics, University of São Paulo (USP), São Paulo, SP, Brazil.

<sup>2</sup>Atmospheric Optics Group of Camagüey. Meteorological Institute of Cuba, Cuba.

<sup>3</sup>Department of Natural and Earth Sciences, Federal University of São Paulo, Diadema, SP, Brazil.

10

11 Correspondence to: Boris Barja Gonzalez (bbarja@gmail.com)

12 **Abstract.** For one year, from July 2011 to June 2012, a ground-based raman lidar provided atmospheric  
 13 observations north of Manaus, Brazil, at an experimental site (2.89°S and 59.97°W) for long-term aerosol  
 14 and cloud measurements. Upper tropospheric cirrus clouds were observed more frequently than previous  
 15 reports in tropical regions. The frequency of occurrence was found to be as high as 82 % during the wet  
 16 season and not lower than 55 % during the dry season. The diurnal cycle shows a minimum around local  
 17 noon and maximum during late afternoon, associated with the diurnal cycle precipitation. Optical and  
 18 geometrical characteristics of these cirrus clouds were derived. The mean values were  $14.4 \pm 2.0$  km  
 19 (top),  $12.7 \pm 2.3$  km (base),  $1.7 \pm 1.5$  km (thickness), and  $0.36 \pm 1.20$  (cloud optical depth). Cirrus clouds  
 20 were found at temperatures down to  $-90$  °C and 7 % were above the tropopause base. The vertical  
 21 distribution was not uniform and two cloud types were identified: (1) cloud base  $> 14$  km and optical  
 22 depth  $\sim 0.02$ , and (2) cloud base  $< 14$  km and optical depth  $\sim 0.2$ . A third type, not previously reported,  
 23 was identified during the wet season, between 16 and 18 km with optical depth  $\sim 0.005$ . The mean lidar  
 24 ratio was  $20.2 \pm 7.0$  sr, indicating a mixture of thick plates and long columns. However, the clouds above  
 25 14 km have a bimodal distribution during the dry season with a secondary peak at about 40 sr suggesting  
 26 that thin plates are a major habit. A dependence of the lidar ratio with cloud temperature (altitude) was  
 27 not found, thus indicating they are well mixed in the vertical. Cirrus clouds classified as subvisible ( $\tau <$   
 28 0.03) were 40 %, whilst 37.7 % were thin cirrus ( $0.03 < \tau < 0.3$ ) and 22.3 % opaque cirrus ( $\tau > 0.3$ ).  
 29 Hence, not only does the central Amazon have a high frequency of cirrus clouds, but a large fraction of  
 30 subvisible cirrus clouds as well. This high frequency of subvisible cirrus clouds may contaminate aerosol  
 31 optical depth measured by sun-photometers and satellite sensors to an unknown extent.

## 1. Introduction

33 Cirrus clouds cover on average more than 30% of the Earth's atmosphere, with higher fractions occurring  
 34 in the Tropics, hence, are important to understanding current climate and predicting future climate (Wylie

*see Marechal 2009  
 40-60%*



et al. 2005, Stubenrauch et al. 2006; Nazaryan et al., 2008). Several studies emphasize the important role that cirrus clouds play in the Earth's radiation budget (i.e. Liou 1986; Lynch et al. 2002; Yang et al. 2010a). Their role is twofold. First, cirrus clouds ~~may~~ increase warming by trapping a portion of infrared radiation emitted by the Earth/atmosphere system. Secondly, cirrus clouds ~~could~~ cool the atmosphere by reflecting part of the incoming solar radiation back into space. The contribution of each effect and the net effect on the radiative forcing depends strongly on cirrus cloud optical properties, altitude, vertical and horizontal coverage (Liou 1986). Therefore, understanding their properties is critical to determining their effect on the albedo and greenhouse effects (Barja and Antuña, 2011, Boucher et al., 2013). Also, ~~the~~ tropical cirrus clouds could influence the vertical distribution of radiative heating in the tropical tropopause layer (e.g., Yang et al., 2010b; Lin et al., 2013). Noticeably, it has been shown that an accurate representation of the cirrus vertical structure in cloud radiative studies improved the results of these calculations (Khvorostyanov and Sassen, 2002; Hogan and Kew, 2005; Barja and Antuña, 2011). Recent research also shows that an increase in stratospheric water vapor are linked mainly with the occurrence of cirrus clouds in the tropical tropopause layer (TTL) (Randel and Jensen, 2013). Finally, measurements of the properties of cirrus clouds at different geographical locations are of utmost importance, potentially allowing for improvements in numerical models parameterizations and, thus, reducing the uncertainties in climatic studies.

DEFINE  
Subsidence  
Cirrus 42

Ground-based lidars are an indispensable tool for monitoring cirrus clouds, particularly identifying optically thin and subvisible cirrus clouds (SVC) with very low optical depth, which are undetectable by cloud radars (Comstock et al., 2002) or by passive instruments (e.g., Ackerman et al., 2008). For this reason, several studies with ground-based lidars have reported the characteristics of cirrus clouds around the globe during the last decade. There are some long-term studies reporting climatologies from midlatitude (eg. Sassen and Campbell, 2001; Goldfarb et al., 2001; Giannakaki et al., 2007; Hoareau et al., 2013) and tropical regions (eg. Comstock et al., 2002; Cadet et al., 2003; Antuña and Barja, 2006; Thorsen et al., 2011; Pandit et al., 2015). Table 1 shows an overview of these studies with different values for cirrus clouds characteristics in diverse geographical regions. There are also some short-term reports on cirrus clouds characteristics during measurement campaigns in midlatitude (e.g. Immler and Schrems, 2002a) and tropical latitudes (Immler and Schrems, 2002b, Pace et al., 2003 and references therein). Additionally, satellite-based measurements have been used to investigate the global distribution of cirrus characteristics (eg. Nazaryan et al., 2008; Sassen et al., 2009; Sassen et al., 2009; Wang and Dessler 2012, Jian et al., 2015). Characteristics of tropical and subtropical cirrus clouds have similar geometrical values and these values are higher than those in midlatitudes. The frequencies of occurrence of cirrus cloud types differ significantly between different locations.

Cirrus cloud~~s~~ measurement~~s~~ reports over tropical rain forests are scarce. Very few global studies with satellites instruments include these regions. Some studies focused on deep convection in the Amazonia reported cirrus clouds (eg. Machado et al., 2002; Hong et al., 2005, Wendisch et al., 2016), but no lidar measurements were used. Baars et al. (2012) focused on aerosol measurements with a ground-based Raman lidar, but report only one cirrus cloud case between 12 km and 16 km during September 11, 2008. Barbosa et al., (2014) describe a week of cirrus clouds measurements from 30 August to 6 September 2011 during an intensive campaign for calibration of the water vapor channel of the UV Raman lidar was



75 conducted in the ACONVEX (Aerosols, Clouds, cONvection EXperiment) site. Cirrus clouds during this  
 76 period were present in 60% of the measurements. Average base and top heights were 11.5 km and  
 77 13.4 km, respectively, and average maximum backscatter occurred at 12.8 km. Most of the time, three  
 78 layers of cirrus clouds were actually found.

79 From the above discussion, the importance of continuous and long-term observations of tropical cirrus  
 80 clouds is evident. In the present study, we use one year of ground-based lidar measurements (July 2011 to  
 81 June 2012) at Manaus, Brazil to investigate the seasonal and diurnal variability of geometrical (cloud top  
 82 and base altitude) and optical (cloud optical depth and lidar ratio) properties of cirrus over a tropical rain  
 83 forest site. In section 2, a brief description of the Raman lidar system, dataset, processing algorithms and  
 84 site are given. The results and discussion are presented in section 3. We close this paper with concluding  
 85 remarks in section 4.

## 86 2. Instrumentation, dataset and algorithms.

### 87 2.1. Site and instrument description

88 The ACONVEX (Aerosols, Clouds, cONvection EXperiment) or T0e (nomenclature of the  
 89 GoAmazon2014/15 experiment sites, Martin et al. 2016) site is located upwind from Manaus-AM,  
 90 Brazil, at 2.89°S and 59.97°W, in the center of the Amazon Forest. ~~The atmospheric observations actually~~  
 91 ~~began in 2011 at this site, and the objective was to operate a combination of several instruments during~~  
 92 ~~the upcoming years for measuring atmospheric humidity, clouds and aerosols, as well as processes which~~  
 93 ~~lead to convective precipitation (Barbosa et al., 2014). Figure 1 gives an overview of the location where~~  
 94 ~~the measurements in this study were done.~~ <sup>were collected</sup> As with most tropical continental sites, the diurnal cycle is  
 95 strong with a late afternoon peak in precipitation (Adams et al., 2013). The usual climatological seasons  
 96 in Central Amazon are: the wet (December to April), dry (July and August), and the transitions wet-to-dry  
 97 (May and June) and dry-to-wet (September to November) (Machado et al., 2004), however the definition ~~s~~  
 98 may vary (e.g. Arraut et al., 2012, Tanaka et al., 2014). Deep convection is a characteristic of the region  
 99 during both seasons, being more active during the wet season (Machado et al., 2002), when it is  
 100 influenced by the intertropical convergence zone (ITCZ). As the ITCZ moves northward during the  
 101 months of dry season, the convective activity decreases. Hence, it is to be expected that deep convection  
 102 is the principal cirrus clouds formation mechanism in the region.

103 The lidar system (LR-102-U-400/HP, manufactured by Raymetrics Advanced Lidar Systems) operates in  
 104 the UV, at 355 nm and has also two Raman channels for nitrogen (387 nm) and water vapor (408 nm).  
 105 The system is tilted from the zenith 5° to avoid specular reflection of horizontally oriented ice crystals. It  
 106 is automatically operated 7 days a week, only being closed between 11 am and 2 pm local time (LT is  
 107 -4 UTC) to avoid the sun crossing the field of view. Detailed information about the lidar system and its  
 108 characterization are given by Barbosa et al. (2014). To retrieve the particle backscatter and extinction  
 109 profiles from the lidar signal, the temperature and pressure profiles were obtained from the radio  
 110 soundings launched at 0 and 12 UTC from the Ponta Pelada Airport, located 28.5 km to the South  
 111 (3.14°S, 59.98°W) of the experimental site.



Defined how?  
 clear-sky SNR  
 or within clouds?

## 112 2.2. Datasets

113 The lidar dataset used in the present study comprises measurements between July 2011 and June 2012. A  
 114 total of 36,597 5-minute profiles were analyzed and only 20,752 had a signal to noise ratio (SNR) higher  
 115 than 3 at the characteristic altitudes of the possible cirrus clouds occurrence (between 8 km and 20 km).  
 116 Statistical tests (not shown) were conducted to obtain the lowest SNR value suitable to detect subvisible  
 117 cirrus clouds, and the value 3 was selected as a threshold for obtaining a good SNR. The number of 5-min  
 118 lidar profiles and number of profiles with good SNR during each month of the studied period were  
 119 analyzed. July, August and September, the driest months (Figure 2) show the higher fraction of profiles  
 120 with good SNR, while the wettest months have the lowest fraction of lidar profiles with good SNR (see  
 121 figure S.1). The cloud fraction of low, optically thick clouds increases during this season, thereby  
 122 attenuating the signal and reaching the cirrus clouds altitudes with a low SNR. The frequency was then  
 123 defined as the ratio between the number of lidar profiles of 5 min with good SNR containing cirrus clouds  
 124 and the total number of profiles with good SNR. This frequency does not count the number of individual  
 125 clouds, but the time coverage of these clouds. Thus, the frequency of occurrence was the best estimate,  
 126 for a ground-based lidar, of the fraction of time when the sky is covered with cirrus clouds of different  
 127 geometric and optical characteristics.

128 Temperature, pressure, geopotential height, humidity and winds for the study period were obtained from  
 129 the ERA Interim reanalysis (Dee et al., 2011) of European Center for Midrange Weather Forecast  
 130 (ECMWF) with spatial resolution of 0.75° and temporal resolution of 6 h. This dataset was used to obtain  
 131 the mean high level winds, near to the cirrus clouds habits (200 hPa). Moreover, the tropopause altitudes  
 132 were obtained from vertical profiles over the site using the methodology of the World Meteorological  
 133 Organization (FCM-H3-1997). A precipitation dataset for the same period was acquired from TRMM  
 134 (Tropical Rainfall Measuring Mission) version 7 product 3B42 (Huffman et al., 2007) with 0.25° and 3 h  
 135 of spatial and temporal resolution, respectively.

## 136 2.3. Cirrus cloud detection algorithm.

137 We used an automatic algorithm for the detection of cloud base, top and maximum backscattering  
 138 heights, based on Barja and Aroche (2001). This algorithm assumes a monotonically decreasing intensity  
 139 of the lidar signal with altitude in a clear atmosphere and searches for significant abrupt changes. These  
 140 abrupt changes are marked as a possible cloud base. Examining the signal noise and the change between  
 141 the possible cloud base, a true cloud base is discriminated. Then, the lowest altitude above cloud base  
 142 with signal lower than that at cloud base and corresponding to a molecular gaseous atmosphere is  
 143 determined as the cloud top. When more than one cloud is present in the same profile, and their top and  
 144 base are separated more than 400 m, they are considered as individual clouds. Figure S.2 gives an  
 145 example of the cloud detection algorithm. Barbosa et al. (2014) provide details on the fully automated  
 146 algorithm, which includes discrimination of false alarm and distinguishing aerosols from thin cloud  
 147 layers. After obtaining the base, top and maximum backscatter heights, the corresponding cloud  
 148 temperatures is obtained from the nearest radiosonde. A detected high cloud is classified as a cirrus cloud  
 149 if the layer has a temperature equal or below than -25°C. These temperatures are reached above 8 km in  
 150 our experimental site almost all the time.

unsure  
 what  
 you  
 are  
 saying

what  
 accommodation  
 did you  
 make for  
 the TTL?

see  
 Campbell  
 et al  
 2015

Uncertainties  
 with ground  
 based cirrus  
 obs

Thorsen et al 2011  
 Protat et al 2014



## 2.4. Cirrus Cloud Optical Depth, backscattering coefficient profile and lidar ratio determination.

The attenuation of the lidar signal by cirrus clouds can be obtained using the ratio of the range corrected signal at the top and at the cloud base as in (Young, 1995):

$$\frac{S(z_t)}{S(z_b)} = \frac{\beta(z_t)}{\beta(z_b)} e^{-2 \int_{z_b}^{z_t} \alpha_p(z') dz'} e^{-2 \int_{z_b}^{z_t} \alpha_m(z') dz'} \quad (1)$$

where  $z_b$  and  $z_t$  are the base and top of cirrus clouds heights,  $S(z) = P(z)z^2$  is the range corrected signal.  $\beta(z)$  and  $\alpha(z)$  are the volumetric backscattering and extinction coefficients, respectively, and each is the sum of a molecular (sub index m) and a particle (sub index p) contribution. Volumetric backscattering and extinction profiles from molecules were derived following Bucholtz (1995). Assuming a negligible aerosol contribution in the atmospheric layers just below and above the cirrus clouds (Young, 1995), we can express the transmittance factor of the lidar equation due to cirrus cloud,  $T^{\text{cirrus}}$ , as

$$T^{\text{cirrus}} = e^{-2 \int_{z_b}^{z_t} \alpha_p(z') dz'} = \frac{S(z_t) \beta(z_b)}{S(z_b) \beta(z_t)} e^{2 \int_{z_b}^{z_t} \alpha_m(z') dz'} \quad (2)$$

And the cirrus optical depth (for an example, see Figure S.2),  $\tau^{\text{cirrus}}$ , as

$$\tau^{\text{cirrus}} = \int_{z_b}^{z_t} \alpha_p(z') dz' = -\frac{1}{2} \ln(T^{\text{cirrus}}) \quad (3)$$

The accuracy of this calculation depends mainly on the SNR at the cirrus cloud altitude. However, when the lidar signal is completely attenuated by the cirrus cloud (i.e. the transmission factor <sup>approaches</sup> goes to zero) it is impossible to obtain the true values of the cirrus top altitude and optical depth. The retrievals, in these cases called apparent values, are necessarily underestimated. ~~Tilting the system by about 5° from the zenith minimizes the effect of the specular reflection on the quasi-horizontal ice crystals.~~

The backscattering coefficients of cirrus clouds were determined by the Fernald-Klett-Sasano method (Fernald et al., 1972; Klett, 1981; Sasano and Nakane, 1984) for each 5-min averaged profile that has large enough SNR above the cirrus cloud, thus allowing a molecular fit. For retrieving the extinction, however, the Klett method requires a predetermined value for the lidar ratio (LR), which is the ratio between the extinction and backscattering coefficients. Then, integrating the extinction coefficient from the cloud base to cloud top, the cirrus cloud optical depth is obtained ( $\tau_{\text{Klett}}^{\text{cirrus}}$ ). Following Chen et al. (2002), we estimated the value of LR for every cloud by iterating over the values of LR and comparing the values of  $\tau_{\text{Klett}}^{\text{cirrus}}$  with the independent value of the cirrus optical depth obtained from the transmittance method described above ( $\tau^{\text{cirrus}}$ ). The cirrus lidar ratio is the one that minimizes the residue:  $R(S) = (\tau_{\text{Klett}}^{\text{cirrus}} - \tau^{\text{cirrus}})^2$ .

The Klett method assumes single scattering, but eventually the received photons could have been scattered by other particles several times before reaching the telescope. This effect, named multiple scattering, increases the laser transmittance and decreases the real extinction coefficient values. Thus, a correction is needed in our calculation of cirrus optical depth. As explained by Chen et al. (2002), for thin clouds it is possible to neglect the multiple scattering effect, nevertheless, we used their proposed correction for all cirrus clouds detected:

$$\eta = \frac{\tau^{\text{cirrus}}}{e^{\tau^{\text{cirrus}} - 1}}; \quad \tau_{\text{corrected}}^{\text{cirrus}} = \frac{\tau^{\text{cirrus}}}{\eta} \quad (4)$$

*punctuation*



*HP = new paragraph*

### 187 3. Results and discussion.

#### 188 3.1. Frequency of cirrus cloud occurrence.

*what is the ~~relative~~ absolute rate of cloud occurrence?*

189 A total of 13,946 lidar profiles were measured with the presence of cirrus clouds, representing a  
 190 frequency of occurrence of 67 % of the total number of profiles with good SNR. Figure 2 shows the  
 191 monthly frequency of occurrence of cirrus clouds in central Amazônia from July 2011 to June 2012, ~~blue~~  
 192 ~~solid line~~. There is a well-defined annual cycle, with maximum values during the months of November,  
 193 December and March, reaching approximately 85 %, and minimum value in August during the dry  
 194 season, but with frequencies no lower than a rather high 50 %. In tropical regions, the main mechanisms  
 195 of cirrus clouds formation are deep convection, large-scale lifting of moist layers, orographic lifting over  
 196 mountain slopes and "cold trapping" near the tropopause (Sassen et al, 2002). Deep convective clouds  
 197 generate cirrus clouds while winds in the upper troposphere removes ice crystals of the top of the large  
 198 convective column, generating the anvil cloud. This cloud remains even after the deep convection cloud  
 199 dissipation and persist from 0.5 to 3 days (Seifert et al, 2007). ~~Due to the huge amount of deep convection~~  
 200 ~~in the Amazon region (Machado et al., 2002, 2014), and the lack of the others formation mechanisms~~  
 201 ~~proposed in the literature (Sassen et al., 2002), e.g. baroclinic fronts and lows and orographic lifting, it is~~  
 202 ~~expected that cirrus clouds are basically formed by this mechanism.~~ However, it should be noted that  
 203 small local topographic effects around Manaus can influence the occurrence and intensity of deep  
 204 convection (Fitzjarrald et al. 2008; Adams et al. 2015). ~~The frequency of deep convection during the~~  
 205 ~~rainy season is higher than the dry season, related with the seasonal change of the Intertropical~~  
 206 ~~Convergence Zone (ITCZ).~~ The boxplot in Figure 2 show the variability of the daily frequency of  
 207 occurrence for each month. There is a high dispersion of the daily frequencies, maximum dispersion in  
 208 August and lowest in November. The monthly cirrus cloud frequency follows the same seasonal pattern  
 209 as the accumulated precipitation (Figure 2, green line), ~~with~~ <sup>with</sup> maximums during the wet months and minimums  
 210 during dry months. For that reason, we divided the study period in wet (January, February, March and  
 211 April), dry (June, July, August and September) and transition (May, October, November and December)  
 212 periods, based on the accumulated precipitation in each month. The average monthly precipitation in  
 213 each season during the observation period was 314 mm, 114 mm and 206 mm respectively.  
 214 The mean wind field on the typical cirrus cloud occurrence altitude (200 hPa) and the precipitation spatial  
 215 distribution during the dry and wet months from July 2011 to June 2012 are shown in the Figure 3.  
 216 During wet months (Figure 3, lower panel), the site is inside the South American Monsoon region with  
 217 great deep convection activity and associated rain ranging from 8 to 14 mm/day on average. Winds at  
 218 200 hPa blow from the southeast ~~at~~ <sup>with</sup> about 20 m/s thus allowing the advection of cirrus clouds produced  
 219 over other parts of the South Atlantic Convergence Zone. As ~~the~~ tropical cirrus can be transported by  
 220 advection thousands of kilometers (Fortuin et al., 2007), we speculate that during the wet period, the  
 221 cirrus clouds observed in central Amazonia are a mixture of locally produced and clouds transported by  
 222 advection from other regions. During the dry period, ~~the convection~~ <sup>convective</sup> activity moved to the north over  
 223 Colombia and Venezuela and the 200 hPa circulation is reversed. Hence, we speculate based on the high  
 224 level circulation and precipitation, that a great contribution to the cirrus clouds observed during the dry  
 225 months is the advection from the other regions.

*These are  
 relative  
 numbers*

*you just  
 said  
 this*

*☆ This is  
 also or  
 implied, tho.  
 The lidar is attenuated  
 otherwise - you are  
 always looking at  
 transport.*



226 The diurnal cycle of the frequency of cirrus clouds is shown in the Figure 4 for the overall period and  
 227 different seasons. All curves exhibit a similar pattern with minimum frequency occurrence values around  
 228 10 and 14 LT hours. Maximum values are found between 17 and 18 LT, in late afternoon, when values  
 229 are slightly higher than in the morning. This diurnal variation of cirrus cloud occurrence follows the  
 230 diurnal cycle of convection and precipitation documented in the literature (e.g. Machado et al., 2002;  
 231 Silva et al., 2011, Adams et al. 2013). Figure 4 shows also the diurnal cycle of precipitation for wet and  
 232 dry months during the study period, averaged over an area of  $2^\circ \times 2^\circ$  centered on the experimental site.  
 233 The maximum of the cycle occurs between 13 and 18 LT, both in dry and wet months, similar to Adams  
 234 et al. (2013). The occurrence of the maximum precipitation in the afternoon coincides with the increase in  
 235 the cirrus frequency in all seasons.  
 236 A larger difference between the maximum and minimum values of the cirrus frequency for the dry  
 237 months is visible in Figure 4. This can be understood by observing the maximum precipitation rates  
 238 during this period, six times lower than those of the wet months, and the upper level circulation (Figure 4)  
 239 that indicates the long range advection. When the frequency of deep convection is greater, close to the  
 240 site, the cirrus clouds are long-lived and more evenly distributed during the day, which does not occur  
 241 during the dry months.

### 242 3.2. Geometrical, optical and microphysical properties of cirrus clouds.

243 Table 2 shows the statistics of the properties of cirrus clouds during the study year and different seasons.  
 244 The overall mean values for the cloud base altitude is  $12.7 \pm 2.3$  km, cloud top is  $14.4 \pm 2.0$  km and  
 245 geometrical thickness is  $1.7 \pm 1.5$  km. The mean value of the cloud maximum backscattering altitude is  
 246  $13.2 \pm 2.3$  km, where the mean temperature is  $-58 \pm 17^\circ\text{C}$ . The differences between the mean values of  
 247 the geometrical properties in different seasons are statistically significant. The frequency of occurrence of  
 248 all cirrus clouds throughout the year was 67 % of the time measurements with good SNR. The seasonal  
 249 behavior discussed previously is also evident, with higher values of frequency of occurrence during the  
 250 wet months (82 %) and lower during dry months (55 %). The mean values of the geometrical  
 251 characteristics are similar, only the thickness is slightly different with 1.9 km (1.6 km) for wet (dry)  
 252 months. Mean COD values are 0.46 and 0.27 for the wet and dry months, respectively. Although the  
 253 similarities between the mean values of the characteristics of all cirrus clouds during both seasons there  
 254 are statistically significant differences between the mean values of the geometrical properties in the  
 255 different seasons.  
 256 Our mean values are similar to those reported by Seifert et al. (2007) in the Maldives ( $4.1^\circ\text{N}$ ,  $73.3^\circ\text{E}$ ):  
 257  $11.9 \pm 1.6$  km (base),  $13.7 \pm 1.4$  km (top),  $1.8 \pm 1.0$  km (thickness),  $12.8 \pm 1.4$  km (max. backscatter) and  
 258  $-58 \pm 11^\circ\text{C}$  (temperature at max. backscatter). Reports from subtropical regions also show similar  
 259 values. Cadet et al. (2003) report for the Reunion Island ( $21^\circ\text{S}$ ,  $55^\circ\text{E}$ ) cirrus cloud base and top altitudes  
 260 of 11 km and 14 km, respectively. Antuña and Barja (2006) report to subtropical experimental site ( $21.4^\circ$   
 261  $\text{N}$ ,  $77.9^\circ\text{W}$ ) cirrus cloud base and top altitudes of 11.63 km and 13.77 km, respectively. On the other  
 262 hand, Sassen and Campbell (2001) show mean values for midlatitude cirrus cloud base/top of 8.79  
 263 km/11.2 km, lower as expected than tropical cirrus and an average geometrical thickness of 1.81 km.  
 264 Some cirrus clouds characteristics reported around the globe are shown in Table 1 for comparison. What

Is this a  
 result  
 of lower  
 SWIR?

defined how?  
 base?  
 top?  
 all layers?  
 Top is  
 most  
 relevant  
 what is  
 absolute  
 frequency  
 of  
 occurrence  
 in  
 your  
 dataset?



See Campbell  
 et al (2016) JAMC-FOZ  
 for similar finding likely  
 = sampling bias

stands out is that our measurements over the Amazon show high frequency of occurrence of subvisible cirrus clouds similar or higher than previously reported from ground-based measurements in the Tropics. The geometrical characteristics of the detected cirrus clouds were examined by means of normalized histograms. Figure 5 shows the results for cloud base and top height, thickness and the corresponding optical depth. Histograms for the wet and dry months reveal differences. The cirrus clouds top altitude distribution (figure 5b), for instance, shows two peaks in the wet months, one centered in 14.25 km and second centered in 17.75 km, with a local minimum centered in 15.25 km and 16.25 km. On the other hand, for dry months, there is only one peak centered at 15.75 km. The local minimum during wet months occurs at 15.25 km, where a higher value near to maximum is found during dry months. For the cloud base (figure 5a), the maximum frequency is in an interval of altitudes around 12.25 km. Similar value of frequency is found in other peak centered at 14.75 km, with local minimum at 14.25 km. There is a local maximum centered in 16.25 km during wet months. For the dry months, this last peak disappears, but the other two peaks remain with higher frequency values and with local minimum at 13.75 km. These results suggest different cirrus types with different origins: cirrus formed directly by anvil outflows from cumulonimbus clouds through local convection; in situ formation from slow large scale air ascent; or possible advection from other convective regions. Comstock et al. (2002) proposed two different types of cirrus clouds at Nauru Island in the tropical western Pacific with oceanic conditions: one type (laminar thin cirrus) with cloud base altitude above 15 km and the other (geometrically thicker and more structured cirrus) with base altitude below this value, with different characteristics. Liu and Zipser (2005) used TRMM Precipitation Radar (PR) dataset to trace the deep convection and precipitation throughout the tropical zone, including oceans and continents. The authors showed that only 1.38 % and 0.1% of tropical convective systems, and consequently their generated cirrus clouds reached 14 km and 16.8 km of altitude, respectively. Hence, they suggested that those clouds with bases about 14 km are the thick anvil type cirrus, and the higher, thin cirrus have their bases above this altitude during the entire study period. Considering these previous results, we suggest that the highest peaks in wet months and the single peak in dry months in cloud base and top histograms have the contribution of cirrus clouds formed far from the site and were transported from large distances. The clouds generated by convective systems can persist in the atmosphere from hours to days if they are slowly lifted (Ackerman et al., 1988; Seifert et al., 2007). Thus, these clouds that ascended and were horizontally transported by long distances are, in general, optically and geometrically thinner and found in upper troposphere and tropical tropopause layer. Our results indeed indicate that these clouds are optically thin. This could be also the reason for which the geometrical thicknesses and optical depth are lower in the dry months see Figure 5 c and d, respectively. We can see that the distribution of the geometrical thickness below 2 km and optical depth below 0.1 in dry months is above the distribution for the wet months. From the cloud base altitude histogram (Figure 5a), one can note the high values for the frequency of occurrence of cloud base heights between 8.5 km and 9.5 km during wet season. This peak is the second most frequent after the principal one centered at 12.25 km and 14.75 km. This secondary peak is a result of using the cloud-base temperature of -25 C as a criterion for defining cirrus clouds. For this altitude,

Base is really meaningful again, this is more implied

DEPENDS where this!!

clouds

NO sample bias



ya think? :)

305 there is possibly a fraction of mixed phase clouds that are counted inadvertently. The most reliable way of  
 306 identifying the cloud phase is by measuring the depolarization caused by backscattered light, not available  
 307 in the present study.

308 Figure 5d shows the normalized histogram of the cirrus clouds optical depth (COD) for the studied period  
 309 and <sup>respective</sup> the wet and dry seasons. In this case, ~~the~~ apparent COD values (explained in section 2) were  
 310 excluded. This histogram shows how ~~the~~ frequency decrease with increases in COD. Moreover, during  
 311 dry months, the cirrus clouds are optically thinner than during wet months.

312 A more in-depth analysis of the vertical distribution of cirrus clouds reveals features of different cirrus  
 313 types, and <sup>its</sup> relation with COD becomes apparent. Figure 6 shows two-dimensional histograms of cloud  
 314 optical depth and cirrus cloud top (upper row) and cloud base (lower row) for the wet months (left  
 315 column) and dry months (right column). During the wet months, there is more dispersion of the values  
 316 than in the dry months, which we speculate might be associated with a larger variability in the outflow  
 317 altitude from deep convective clouds. The cloud-base distributions (Figure 6c, d) clearly show that the  
 318 higher values of COD correspond to lower cloud base, whereas the lower values correspond to higher  
 319 cloud base. The almost linear decrease is steeper for wet months (Figure 6c) than dry months (Figure 6d).

320 Hence, cirrus with the same cloud base altitude are more optically thick during that period. There are two  
 321 maxima during the dry months, suggesting two types of cirrus clouds, those with bases below and those  
 322 with bases above 13.75 km. The low altitude type has a cloud base at about 12.25 km and COD 0.20,  
 323 while the high altitude ones, have a base at 14.75 km and subvisible optical depths of 0.01. During wet  
 324 season, the two groups are much less pronounced and have higher COD. These cirrus clouds types were  
 325 previously reported for the tropical region by Comstock et al. (2002) and Pace et al. (2003). However, the  
 326 altitude that separates these two types of clouds over the Amazon (13.75 km) is lower than that reported  
 327 over Nauru Island in the tropical western Pacific (15 km) by Comstock et al. (2002) and over Mahé Island  
 328 in the tropical Indian Ocean (14.50 km) by Pace et al. (2003). Moreover, we also identified another group  
 329 of subvisible clouds with very high cloud base (16.25 km) during the wet months, which is likely above  
 330 the tropopause.

331 In the case of cloud top, the relation with COD is not clear. During the dry months (Figure 6b), almost all  
 332 cirrus clouds tops, regardless of their COD, are found around 16.75 km. During the wet months, the cloud  
 333 tops are spread from 13 km to 16 km, but all COD values occur at all altitudes. To investigate the role of  
 334 the tropopause capping on the cirrus vertical development, its altitude was calculated from the ERA  
 335 Interim dataset (see section 2). The tropopause mean altitudes during the wet, transition and dry periods  
 336 are  $16.5 \pm 0.2$  km,  $16.3 \pm 0.3$  and  $15.9 \pm 0.4$ , respectively.

337 Figure 7 shows the distribution of the distance from the cloud top and bottom to the tropopause. About  
 338 7 % (22 %) of the detected cirrus clouds have cloud base (top) above the tropopause during the wet  
 339 season, and 6 % (17 %) during the dry season. Most of the cirrus clouds tops are found right below the  
 340 tropopause inversion (see figure S.3a and S.3b), except during the wet season when they are found from -  
 341 3 km to +0.5 km. The presence of the cirrus clouds in the tropical tropopause layer is the consequence of  
 342 ~~the~~ deep and strong convection in the Amazonian region, reported previously by Liu and Zipser (2009).  
 343 Their vertical distribution can then be understood as following. During the wet season, the intensity of  
 344 deep convection in central Amazonia (as measured with convective available potential energy, water

See  
 Campbell  
 et al  
 2015  
 Berry and  
 Mull 2014

< cool

TTL  
 RIGHT = nucleating level, which  
 is independent  
 of vertical  
 extent and  
 COD

Again, this  
 is confusing  
 with respect  
 to how the  
 TTL is defined



345 vapor convergence, cloud top temperatures) can vary (Machado et al., 2002; Adams et al., 2009, 2013,  
 346 2015). Moreover, the tropopause is higher during the wet season (figure S.3c). Hence the cloud tops can  
 347 be found from 13 km to 18 km, and cloud bases from 9 km to 18 km (figure 6). During the dry season,  
 348 deep convection is found primarily north of the equator (figure 3), hence the cirrus clouds measured at  
 349 Manaus are mostly those transported over long distances by the prevailing winds (figure 3). As the cirrus  
 350 produced northward around the tropopause do not last long, as they cannot be adiabatically lifted (Jensen  
 351 et al., 1996), they do not reach the measurement site and there is only one maximum near 15 km in the  
 352 distribution of cloud tops. During these dry months over the Amazon, however, precipitation is still about  
 353 100 mm per month. Hence, there is a second type of cirrus clouds (Figure 7a and 6d), which those are  
 354 produced nearby, and hence are lower and optically thicker.

355 The statistical characteristics of cirrus clouds above and below 14 km are shown in the Table 2. Mean  
 356 values of the properties are different for these cloud types. Cirrus clouds above 14 km are geometrical and  
 357 optically thinner than clouds below 14 km. There are statistically significant differences between the  
 358 properties of these two cirrus clouds types and between seasons. Also, there is a seasonal behaviour of the  
 359 of these cloud types. During wet months the cirrus clouds are higher and optical and geometrically thicker  
 360 than during the dry months.

361 The classification of cirrus clouds following Sassen and Cho (1992) shows that 40.0 % of the cirrus  
 362 clouds measured in our experimental site are subvisible ( $\tau < 0.03$ ), 37.7 % are thin cirrus ( $0.03 < \tau < 0.3$ )  
 363 and 22.3 % are opaque cirrus ( $\tau > 0.3$ ). Table 2 shows these values for each season. subvisible cirrus  
 364 clouds have the highest (lower) fraction during dry (wet) months. Opaque clouds have the highest (lower)  
 365 fraction during wet (dry) months which is expected as there is a dominance of newly generated clouds by  
 366 deep convection columns. This large fraction of optically thin and subvisible cirrus clouds over the

367 Amazon present a challenge for using passive remote sensing from space, such as MODIS. As mentioned  
 368 by Ackerman et al. (2010), thin cirrus clouds are difficult to detect because of insufficient contrast with  
 369 the surface radiance. MODIS only detects cirrus with optical depth higher than 0.2 (Ackerman et al.,  
 370 2008). Therefore, the MODIS's cloud-mask does not include 71 % of cirrus clouds over the Amazon, and  
 371 likewise, their estimation of aerosol optical depth might be contaminated with these thin cirrus. Aerosol  
 372 optical depth measurements from AERONET can also be contaminated with thin cirrus clouds. Chew et  
 373 al. (2011), for instance, estimated a contamination of about 0.034 to 0.060 in AERONET AOD in  
 374 Singapore, where the cirrus frequency of occurrence is about 34%. Therefore, in our region with much  
 375 higher cirrus frequency, the AERONET AOD might be more contaminated. Exactly how much  
 376 contamination from thin cirrus there might be in MODIS and AERONET aerosol products over the  
 377 Amazon will be the subject of a forthcoming study.

378 These different types of cirrus clouds measured in central Amazonia, with different formation  
 379 mechanisms, optical depths and altitude range are expect to be composed of ice crystals of different  
 380 shapes. One way to gain information is to compute the ratio of the backscatter to the total extinction, the  
 381 so-called lidar-ratio. As explained in section 2, we are able to find the average lidar-ratio for the detected  
 382 cirrus clouds using an interactive approach instead of explicitly calculating the extinction from the Raman  
 383 signal, which would be available only during night-time. Figure 8 shows the histograms of lidar ratio  
 384 values for cirrus clouds during dry and wet months. The cirrus clouds were divided in three categories,

How?

you really  
 don't  
 know  
 this

consistent  
 with  
 Campbell  
 et al 2016  
 JAMC  
 EOR

Chew et al.

no

Awesome



385 following our previous discussion: those clouds with base above 14 km, top below 14 km and those with  
 386 top (base) above (below) 14 km. In all case, the most frequent lidar ratios are between 16 sr and 20 sr.  
 387 There are notable differences only for the distributions for higher clouds (base above 14 km) during dry  
 388 months, when we observed two types of cirrus (Figure 6). For dry months, there is a large frequency of  
 389 occurrence of cirrus clouds with lidar ratios around 40 sr. According to the study of Sassen et al. (1989),  
 390 cirrus clouds composed of thick plates, long columns and thin plates would have lidar ratio values around  
 391 11.6 sr, 26.3 sr and 38.5 sr, respectively. Hence, during wet months there is the predominant mixture of  
 392 thick plates and long columns for all clouds. During dry months, the cirrus clouds that are entirely above  
 393 14 km have an important contribution of thin plates. These are long-range transported cirrus, thus the  
 394 aged ice crystals, will tend to become thinner during the transport.  
 395 The mean value of  $20.2 \pm 7.0$  sr is obtained for the whole period and varying less than 1.5 sr for different  
 396 season months. Pace et al., (2003) showed a distribution to the inverse value of lidar ratio similar to that  
 397 presented here. They found a mean value of lidar ratio of 19.6 sr for the tropical site of Mahé, Seychelles.  
 398 Seifert et al. (2007), also for tropical regions report values near to 32 sr. Platt and Diley, (1984) reported  
 399 the value of 18.2 sr with an error of 20%. The value of the lidar ratio may vary greatly depending on the  
 400 altitude and composition of cirrus clouds (Goldfarb et al., 2011). For the other latitudes, there are  
 401 differences between the lidar ratio values examples given in Table 1.  
 402 After the analysis of the properties of the cirrus clouds it is interesting to examine the behavior of the  
 403 variable with the temperature. Figure 9 show the dependence of the geometrical thickness, optical depth  
 404 and lidar ratios with the cirrus clouds temperature. The plots show temperature uniform intervals of  
 405 2.5 °C, and the variables with their mean and standard deviation for each corresponding interval. The  
 406 upper and middle panels contain the dependence of the geometrical thickness and optical depth with  
 407 cloud base temperature, respectively. We can see both variables increase at higher temperatures. Values  
 408 nearly to 3 km of geometrical thickness and 0.9 optical depth correspond to a temperature of -25 °C,  
 409 decreasing monotonically for lower temperatures in both month's periods. Similar results are reported by  
 410 Hoareau et al. (2013) and Seifert et al. (2007).  
 411 The lower panel in Figure 9 shows the dependence between lidar ratio with mid-level cloud temperature. A  
 412 slight increase in the lidar ratio values from 15 sr to 24 sr when the temperature decrease up to -70 °C is  
 413 showed for dry period. During the wet period, the lidar ratio values are between 15 sr and 20 sr in all  
 414 temperature intervals. Seifert et al. (2007) and Pace et al. (2003) both show the same temperature  
 415 dependence of the lidar ratio, but with different mean values of lidar ratio. This behavior is an indication  
 416 of little variation in the microphysical characteristics of observed clouds. Nevertheless, for the dry period,  
 417 the lidar ratio grows when temperatures are below -75 °C. These temperature intervals correspond to the  
 418 clouds above 14 km discussed previously. These clouds above 14 km have different ice crystals shapes  
 419 concluded from the analysis of the right panel from Figure 9.

How did you  
 derive the  
 uncertainty?  
 Standard  
 deviation?

See  
 Garnier  
 et al  
 2015  
 AMT

why mid-  
 level  
 you're likely  
 attenuated

#### 420 4. Conclusions.

421 The ACONVEX site started in 2011 with the goal of continuously monitoring climate relevant cloud  
 422 properties in central Amazonia. The ground based lidar measurements from July 2011 to June 2012 were  
 423 used to investigate the geometrical and optical properties of cirrus clouds in the region. An algorithm was



*Relative gravity when you had  
 enough to  
 SUR?*

424 developed to search through this dataset with high vertical and temporal resolution and to automatically  
 425 find the clouds, calculate the particle backscatter, and derive the optical depth and lidar-ratio. The  
 426 frequency of occurrence during the observation period was 67 %, which is higher than all previous reports  
 427 in the literature for other tropical regions. This frequency reached 82 % during the wet months (January,  
 428 February, March and April), but decreased to 55 % during the dry months (June, July, August, and  
 429 September). The analysis of high-level circulation and precipitation during the dry months indicate that  
 430 advection from the northern regions is likely the main source of these cirrus. ~~While~~ <sup>What</sup> during the wet  
 431 period, there was a mixture of locally produced and advected clouds. However, the diurnal cycle of the  
 432 frequency of cirrus clouds showed a minimum around 12h LT and maximum around 18h LT, following  
 433 the diurnal cycle of the precipitation for both seasons. *~ SUR?*

434 The geometrical, optical and microphysical characteristics of cirrus clouds measured in the present study  
 435 were consistent and in agreement with other reports from tropical regions. The mean values were  
 436  $12.7 \pm 2.3$  km (base),  $14.4 \pm 2.0$  km (top),  $1.7 \pm 1.5$  km (thick), 0.36 (optical depth) and 20.2 sr (lidar  
 437 ratio). With the exception of the optical depth and lidar ratio, these mean values are similar to those found  
 438 during the wet, transition and dry periods. Cirrus clouds were found at temperatures up to  $-90$  °C and 7 %  
 439 of the cirrus were above the tropopause level or in the tropical tropopause layer. ~~The role of these clouds~~  
 440 ~~in wetting or drying the stratosphere was left for another study.~~

441 By simultaneously analyzing cloud altitude and COD, it was found that cirrus clouds during the dry  
 442 months are optically thinner and lower in altitude than those during the wet period. Moreover, the higher  
 443 values of COD correspond to lower cloud base, whereas the lowest values, to higher cloud base. The  
 444 almost linear decrease is steeper for wet months than dry months, hence, cirrus with the same cloud base  
 445 altitude are more optically thick during wet season. The statistical distribution of altitude and COD  
 446 suggested the presence of two cloud types as expected. The first is located above 14 km with COD ~  
 447 0.02, and the second type at lower altitudes with COD ~ 0.2. A third type, not previously reported, was  
 448 identified during the wet season, between 16 and 18 km with COD ~ 0.005. Cirrus clouds above 14 km  
 449 were geometrically and optically thinner than those below, but have higher lidar ratios.

450 For the first time, the lidar ratio of cirrus clouds was obtained for this region. The mean lidar ratio was  
 451  $20.2 \pm 7.0$  sr, indicating a mixture of thick plates and long columns ice crystals, in agreement with other  
 452 reports from the tropical regions. The statistical distribution of lidar ratios measured in the different  
 453 seasons is the same, and they also do not vary with the temperature (altitude) of the cirrus clouds,  
 454 indicating that these clouds are well mixed in the vertical. It was observed, however, that the distribution  
 455 of the lidar ratio for clouds above 14 km during dry months shows a secondary peak around 40 sr,  
 456 suggesting a different crystal shape like thin plates. From all cirrus clouds observed, 40 % were classified  
 457 as subvisible (COD < 0.03), 38 % were as thin ( $0.03 < \text{COD} < 0.3$ ) and 22 % as opaque (COD > 0.3).  
 458 During the dry months, the subvisible cirrus clouds reached a maximum of 46 %, while opaque cirrus has  
 459 their maximum during wet months. These values are characteristic for our region and slightly different  
 460 from measurements in other tropical regions. The central Amazon has a high frequency of cirrus clouds in  
 461 general, and a large fraction of subvisible cirrus clouds. Therefore, the aerosol optical depth determined  
 462 by sun-photometers and satellite based sensor in this region might be contaminated with the COD of these



463 thin clouds. Future work must be conducted in order to evaluate how large this contamination might be  
 464 over the Amazon.

## 465 5. Acknowledgements

466 We thank the researcher David K Adams from UNAM for reviews and valuable comments to improve the  
 467 paper content. We acknowledge the financial support from CAPES project A016\_2013 on the program  
 468 Science without Frontiers, FAPESP Research Program on Global Climate Change under research grants  
 469 2008/58100-1, 2009/15235-8, 2012/16100-1, 2013/50510-5, and 2013/05014-0. Maintenance and  
 470 operation of the instruments at the experimental site would not have been possible without the  
 471 institutional support from EMBRAPA. We thank INPA, The Brazilian Institute for Research in Amazonia  
 472 and the LBA Central office for logistical support. Special thanks to Marcelo Rossi, Victor Souza and  
 473 Jocivaldo Souza at Embrapa, and to Ruth Araujo, Roberta Souza, Bruno Takeshi and Glauber Cirino from  
 474 LBA.

## 475 6. References

- 476 Ackerman, S., Holz, R., Frey, R., and Eloranta, E.: Cloud Detection with MODIS: Part II Validation, J  
 477 Atmos Oceanic Tech, 25(1073-1086), doi:DOI:10.1175/2007JTECHA1053.1, 2008.
- 478 Ackerman, S., Frey, R., Strabala, K., Liu, Y., Gumley, L., Baum, B., Menzel, P.: Discriminating Clear-  
 479 Sky From Cloud With MODIS. Algorithm Theoretical Basis Document (MOD35). ATBD Version  
 480 6.1. October 2010. 2010.
- 481 Adams, D. K., Souza, E., and Costa, A.: Moist Convection in Amazonia: Implications for Numerical  
 482 Modeling (in Portuguese). Revista Brasileira de Meteorologia, 13, 168-178, 2009.
- 483 Adams, D. K., Gutman, S. I., Holub, K. L., and Pereira, D. S.: GNSS observations of deep convective  
 484 time scales in the Amazon. Geophysical Research Letters, 40, 2818-2823, 2013.
- 485 Adams, D. K., Fernandes, R. M. S., Holub, K. L., Gutman, S. I., Barbosa, H. M. J., Machado, L. A. T.,  
 486 Calheiros, A. J. P., Bennett, R. A., Kursinski, E. R., Sapucci, L. F., DeMets, C., Chagas, G. F. B.,  
 487 Arellano, A., Filizola, N., Amorim Rocha, A. A., Araújo Silva, R., Assunção, L. M. F., Cirino, G.  
 488 G., Pauliquevis, T., Portela, B. T. T., Sá, A., de Sousa, J. M., and Tanaka, L. M. S: The Amazon  
 489 Dense GNSS Meteorological Network: A New Approach for Examining Water Vapor and Deep  
 490 Convection Interactions in the Tropics. Bull. Amer. Meteor. Soc., 96, 2151–2165, 2015.
- 491 Antuña, J. C. and Barja, B.: Cirrus cloud optical properties measured with lidar in Camagüey, Cuba,  
 492 Óptica Pura y Aplicada, 39, 11–16, 2006.
- 493 Arraut, J.M., Nobre, C.A., Barbosa, H.M.J., Marengo J.A., and Obregon, G.: Aerial Rivers and Lakes:  
 494 looking at large scale moisture transport, its relation to Amazonia and to Subtropical Rainfall in  
 495 South America, J. Climate, 25, pp. 543-556, doi: 10.1175/2011JCLI4189.1, 2012.
- 496 Baars, H., Ansmann, A., Althausen, D., Engelmann, R., Heese, B., Müller, D., Artaxo, P., Paixao, M.,  
 497 Pauliquevis, T., and Souza, R.: Aerosol profiling with lidar in the Amazon Basin during the wet  
 498 and dry season, J. Geophys. Res., 117, D21201, 2012.doi:10.1029/2012JD018338, 2012.
- 499 Barja, B., Aroche, R.: Cirrus clouds at Camagüey, Cuba, Proceedings of the SPARC 2000, 2001.



- 500 Barja, B. and Antuña, J. C.: The effect of optically thin cirrus clouds on solar radiation in Camagüey,  
501 Cuba, Atmos. Chem. Phys., 11, 8625–8634, doi:10.5194/acp-11-8625-2011, 2011.
- 502 Barbosa, H. M. J., Pauliquevis, T., Adams, D. K., Artaxo, P., Cirino, G., Barja, B., Correia, A., Gomes,  
503 H., Gouveia, D. A., Padua, M. B., Rosario, N. M. E., Souza, R. A. F., Santos, R. M. N., Sapucci,  
504 L., and Portela, B. T.: ACONVEX—Aerosols, Clouds, cONvection, Experiment—A new site in  
505 central Amazonia for long term monitoring of aerosol-clouds-convection interactions. In: AMS  
506 95th Annual Meeting Proceedings – Phoenix, Arizona, January 2015, 2015.
- 507 Barbosa, H. M. J., Barja, B., Pauliquevis, T., Gouveia, D. A., Artaxo, P., Cirino, G. G., Santos, R. M. N.,  
508 and Oliveira, A. B.: A permanent Raman lidar station in the Amazon: description, characterization,  
509 and first results, Atmos. Meas. Tech., 7, 1745–1762, doi:10.5194/amt-7-1745-2014, 2014.
- 510 Boucher, O., Randall, D., Artaxo, P., Bretherton, C., Feingold, G., Forster, P., Kerminen, V.-M., Kondo,  
511 Y., Liao, H., Lohmann, U., Rasch, P., Satheesh, S.K., Sherwood, S., Stevens, B., and Zhang, X.Y.:  
512 Clouds and Aerosols. In: Climate Change 2013: The Physical Science Basis. Contribution of  
513 Working Group I to the Fifth Assessment Report of the Intergovernmental Panel on Climate  
514 Change [Stocker, T.F., D. Qin, G.-K. Plattner, M. Tignor, S.K. Allen, J. Boschung, A. Nauels, Y.  
515 Xia, V. Bex and P.M. Midgley (eds.)]. Cambridge University Press, Cambridge, United Kingdom  
516 and New York, NY, USA, 2013.
- 517 Bucholtz, A.: Rayleigh-scattering calculations for the terrestrial atmosphere, Applied Optics 34, 2765–  
518 2773, 1995.
- 519 Cadet, B., Goldfarb, L., Faduilhe, D., Baldy, S., Giraud, V., Keckhut, P., and Réchou, A.: A sub-tropical  
520 cirrus clouds climatology from Reunion Island (21°S, 55°E) lidar data set, Geophys. Res. Lett.,  
521 30(3), 1130, doi:10.1029/2002GL016342, 2003.
- 522 Chen, W.; Chiang, C.; Nee, J.: Lidar ratio and depolarization ratio for cirrus clouds. Applied Optics, v.  
523 41, n. 30, p. 6470–6476, 2002.
- 524 Chew B, Campbell J, Reid J, Giles D, Welton E, Salinas S, Liew S.: Tropical cirrus cloud contamination  
525 in sun photometer data. Atmospheric Environment;45 (37):6724–6731, 2011.
- 526 Comstock, J. M., Ackerman, T. P., and Mace, G. G.: Ground-based lidar and radar remote sensing of  
527 tropical cirrus clouds at Nauru Island: Cloud Statistics and radiative impacts, J. Geophys.  
528 Res., 107, 4714, doi:10.1029/2002JD002203, 2002.
- 529 Dupont, J.-C., Haeffelin, M., Morille, Y., Noël, V., Keckhut, P., Winker, D., Comstock, J., Chervet, P.,  
530 and Roblin, A.: Macrophysical and optical properties of midlatitude cirrus clouds from four  
531 ground-based lidars and collocated CALIOP observations, J. Geophys. Res., 115, D00H24,  
532 doi:10.1029/2009JD011943, 2010.
- 533 Elouragini, S., and Flamant, P. H.: Iterative method to determine an averaged backscatter-to-extinction  
534 ratio in cirrus clouds”, Applied Optics, 35, Issue 9, pp. 1512–1518, 1996.
- 535 FCM-H3-1997: Rawinsonde and Pibal Observations, Federal Meteorological Handbook No. 3,  
536 <http://www.ofcm.gov/fmh3/text/rawinson.htm>, 1997
- 537 Fernald, F. G., Herman, B. M. and Reagan, J. A.: Determination of aerosol height distribution by lidar,  
538 Appl. Opt., 11, 482–489, 1972.



- 539 Fitzjarrald, D. R., Sakai, R. K., Moraes, O. L. L., de Oliveira, R. C., Acevedo, O. C., Czikowsky, M. J.,  
 540 and Beldini, T.: Spatial and temporal rainfall variability near the Amazon-Tapajós confluence. *J.*  
 541 *Geophys. Res.*, 113, G00B11, doi:10.1029/2007JG000596, 2008.
- 542 Fortuin, J. P. F., Becker, C. R., Fujiwara, M., Immmler, F., H. M. Kelder, Scheele, M. P., and Schrems, O.,  
 543 Verver, G. H. L.: Origin and transport of tropical cirrus clouds observed over Paramaribo,  
 544 Suriname (5.8°N, 55.2°W), *J. Geophys. Res.*, 112, D09107, doi:10.1029/2005JD006420, 2007.
- 545 Giannakaki, E., Balis, D. S., Amiridis, V., and Kazadzis, S.: Optical and geometrical characteristics of  
 546 cirrus clouds over a Southern European lidar station, *Atmos. Chem. Phys.*, 7, 5519–5530,  
 547 doi:10.5194/acp-7-5519-2007, 2007.
- 548 Goldfarb, L., Keckhut, P., Chanin, M.-L., and Hauchecorne, A.: Cirrus climatological results from lidar  
 549 measurements at OHP (44° N, 6° E), *Geophys. Res. Lett.*, 28, 1687–1690, 2001.
- 550 Hoareau, C., Keckhut, P., Noel, V., Chepfer, H., and Baray, J.-L.: A decadal cirrus clouds climatology  
 551 from ground-based and spaceborne lidars above the south of France (43.9° N–5.7° E), *Atmos.*  
 552 *Chem. Phys.*, 13, 6951–6963, doi:10.5194/acp-13-6951-2013, 2013.
- 553 Hogan, R. J., and Kew, S. F.: A 3D stochastic cloud model for investigating the radiative properties of  
 554 inhomogeneous cirrus clouds. *Q. J. R. Meteorol. Soc.*, 131, 2585–2608, 2005.
- 555 Hong, G., Heygster, G., Miao, J., and Kunzi, K.: Detection of tropical deep convective clouds from  
 556 AMSU-B water vapor channels measurements, *J. Geophys. Res.*, 110, D05205,  
 557 doi:10.1029/2004JD004949, 2005.
- 558 Huffman, G.J., Adler, R.F., Bolvin, D.T., Gu, G., Nelkin, E.J., Bowman, K.P., Hong, Y., Stocker, E.F.,  
 559 and Wolff, D.B.: The TRMM multi-satellite precipitation analysis: quasi-global, multi-year,  
 560 combined-sensor precipitation estimates at fine scale. *J. Hydrometeorol.* 8 (1), 38–55, 2007.
- 561 Immmler, F. and Schrems, O.: LIDAR measurements of cirrus clouds in the northern and southern  
 562 midlatitudes during INCA (55° N, 53° S): A comparative study, *Geophys. Res. Lett.*, 29, 1809,  
 563 doi:10.1029/2002GL015076, 2002a.
- 564 Immmler, F., and Schrems, O.: Determination of tropical cirrus properties by simultaneous LIDAR and  
 565 radiosonde measurements, *Geophys. Res. Lett.*, 29/23, 4, doi:10.1029/2002GL015076, 2002b.
- 566 Jensen, E. J., Toon, O. B., Selkirk, H. B., Spinhirne, J. D., and Schoeberl, M. R.: On the formation and  
 567 persistence of subvisible cirrus clouds near the tropical tropopause, *J. Geophys. Res.*, 101(D16),  
 568 21361–21375, doi:10.1029/95JD03575, 1996.
- 569 Jiang, J; H., Su, H., Zhai, Ch., Shen, T. J., Wu, T., Zhang, J., Cole, J. N. S., von Salzen, K., Donner, L. J.,  
 570 Seman, Ch., Del Genio, A., Nazarenko, L. S., Dufresne, J.-L., Watanabe, M., Morcrette, C.,  
 571 Koshiro, T., Kawai, H., Gettelman, A., Millán, L., Read, W.G., Livesey, N. J., Kasai, Y., and  
 572 Shiotani, M.: Evaluating the Diurnal Cycle of Upper-Tropospheric Ice Clouds in Climate Models  
 573 Using SMILES Observations. *J. Atmos. Sci.*, 72, 1022–1044. doi:10.1175/JAS-D-14-0124.1,  
 574 2015.
- 575 Kärcher, B.: Cirrus clouds in the tropical tropopause layer: Role of heterogeneous ice nuclei, *Geophys.*  
 576 *Res. Lett.*, 31, L12101, doi:10.1029/2004GL019774, 2004.



- 577 Khvorostyanov, V. I., and Sassen, K.: Microphysical processes in cirrus and their impact on radiation A  
 578 Mesoscale Modeling Perspective, in Cirrus ed D Lynch, K Sassen, D O C Starr and G Stephens  
 579 (Oxford: Oxford University Press) pp 397–432, 2002.
- 580 Kim, Y., Kim, S.-W., Kim, M.-H. and Yoon, S.-C.: Geometric and optical properties of cirrus clouds  
 581 inferred from three-year ground-based lidar and CALIOP measurements over Seoul, Korea,  
 582 Atmospheric Research, 139, 27-35, 2014.
- 583 Klett, J.D.: Stable analytical inversion solution for processing lidar returns. Appl. Opt. 20(2), 211–220,  
 584 1981.
- 585 Lakkis, G.S., Lavorato, M., and Canziani, O.P.: Monitoring cirrus clouds with lidar in the Southern  
 586 Hemisphere: a local study over Buenos Aires. 1. Tropopause heights. Atmos. Res. 92 (1), 18–26,  
 587 2009.
- 588 Lin, L., Fu, Q., Zhang, H., Su, J., Yang, Q., and Sun, Z.: Upward mass fluxes in tropical upper  
 589 troposphere and lower stratosphere derived from radiative transfer calculations, J. Quant.  
 590 Spectrosc. Radiat. Transfer, 117, 114–122, 2013.
- 591 Liou, K. N.: Influence of cirrus clouds on weather and climate processes: A global perspective. Mon.  
 592 Wea. Rev., 114, 1167–1199, 1986.
- 593 Liu, C., and Zipser, E. J.: Implications of the day versus night differences of water vapor, carbon  
 594 monoxide, and thin cloud observations near the tropical tropopause, J. Geophys. Res., 114,  
 595 D09303, doi:10.1029/2008JD011524, 2009.
- 596 Lynch, D. K., Sassen, K., Starr, D. O., and Stephens, G.: Cirrus. Oxford University Press, 480 pp., 2002.
- 597 Machado, L.A.T., Laurent, H., and Lima, A.A.: Diurnal march of the convection observed during  
 598 TRMM-WETAMC/LBA, J. Geophys. Res., 107(D20), 8064, doi:10.1029/2001JD000338, 2002.
- 599 Machado, L.A.T.; Laurent, H.; Dessay, N.; Miranda, I.: Seasonal and diurnal variability of convection  
 600 over the Amazonia - A comparison of different vegetation types and large scale forcing.  
 601 Theoretical and Applied Climatology, 78, 61-77, doi: 10.1007/s00704-004-0044-9. 2004.
- 602 Machado, L.A.T., Silva Dias, M.A.F., Morales, C., Fisch, G., Vila, D., Albrecht, R., Goodman, S.J.,  
 603 Calheiros, A.J.P., Biscaro, T., Kummerow, C., Cohen, J., Fitzjarrald, D., Nascimento, E.L.,  
 604 Sakamoto, M.S., Cunningham, C., Chaboureaud, J. -P., Petersen, W.A., Adams, D.K., Baldini, L.,  
 605 Angelis, C.F., Sapucci, L.F., Salio, P., Barbosa, H.M.J., Landulfo, E., Souza, R.A.F., Blakeslee,  
 606 R.J., Bailey, J., Freitas, S., Lima, W.F.A., Tokay, A.: THE CHUVA PROJECT: how does  
 607 convection vary across Brazil? Bull. Am. Meteor. Soc., 1365–1380, doi:10.1175/BAMS-d-13-  
 608 00084.1, 2014.
- 609 Martin, S. T., Artaxo, P., Machado, L. A. T., Manzi, A. O., Souza, R. A. F., Schumacher, C., Wang, J.,  
 610 Andreae, M. O., Barbosa, H. M. J., Fan, J., Fisch, G., Goldstein, A. H., Guenther, A., Jimenez, J.  
 611 L., Pöschl, U., Silva Dias, M. A., Smith, J. N., and Wendisch, M.: Introduction: Observations and  
 612 Modeling of the Green Ocean Amazon (GoAmazon2014/5), Atmos. Chem. Phys., 16, 4785–4797,  
 613 doi:10.5194/acp-16-4785-2016, 2016.
- 614 Nazaryan, H., McCormick, M. P., and Menzel, W. P.: Global characterization of cirrus clouds using  
 615 CALIPSO data, J. Geophys. Res., 113, D16211, doi:10.1029/2007JD009481, 2008.



- 616 Pace, G., Cacciani, M., di Sarra, A., Fiocco, G., and Fuà, D.: Lidar observations of equatorial cirrus  
 617 clouds at Mahé Seychelles, *J. Geophys. Res.*, 108(D8), 4236, doi:10.1029/2002JD002710, 2003.
- 618 Pandit, A. K., Gadhave, H. S., Venkat Ratnam, M., Raghunath, K., Rao, S. V. B., and Jayaraman, A.:  
 619 Long-term trend analysis and climatology of tropical cirrus clouds using 16 years of lidar data set  
 620 over Southern India. *Atmos. Chem. Phys.*, 15, 13833–13848, doi:10.5194/acp-15-13833-2015,  
 621 2015
- 622 Quante, M., and Starr, D. O'C.: Dynamical processes in cirrus clouds: Review of observational results.  
 623 Chapter 17 in: D. Lynch, K. Sassen, D.O'C. Starr, G. Stephens (eds.): *Cirrus*. Oxford University  
 624 Press, New York, 346-374, 2002.
- 625 Randel, W. J. and Jensen, E. J.: Physical processes in the tropical tropopause layer and their roles in a  
 626 changing climate, *Nat. Geosci.*, 6, 169–176, doi:10.1038/ngeo1733, 2013.
- 627 Sasano Y., and Nakane H.: Significance of the extinction/backscatter ratio and the boundary value term in  
 628 the solution for the two-component lidar equation", *Appl. Opt.*, vol. 23, 11–13, 1984.
- 629 Sassen, K., Starr, D. O'C., and Uttal, T.: Mesoscale and Microscale Structure of Cirrus Clouds: Three  
 630 Case Studies, *J of the Atmos. Sci.* 46:3, 371-396, 1989.
- 631 Sassen, K. and Campbell, J. R.: A midlatitude cirrus cloud climatology from the facility for atmospheric  
 632 remote sensing. Part I: Macrophysical and synoptic properties, *J. Atmos. Sci.*, 58, 481–496, 2001.
- 633 Sassen, K.: Cirrus Clouds. A Modern Perspective, In *Cirrus* D. Lynch, K. Sassen, D. O'C Starr, and G.  
 634 Stephens Eds., Oxford University Press, 136-146, 2002.
- 635 Sassen, K., Wang, Z., and Liu, D.: Global distribution of cirrus clouds from CloudSat/Cloud-Aerosol  
 636 Lidar and Infrared Pathfinder Satellite Observations (CALIPSO) measurements, *J. Geophys. Res.*,  
 637 113, D00A12, doi:10.1029/2008JD009972, 2008.
- 638 Sassen, K., Wang, Z., and Liu, D.: Cirrus clouds and deep convection in the tropics: Insights from  
 639 CALIPSO and CloudSat, *J. Geophys. Res.*, 114, D00H06, doi:10.1029/2009JD011916, 2009.
- 640 Seifert, P.; Ansmann, A.; Müller, D.; Wandinger, U.; Althausen, D.; Heymsfield, A. J.; Massie, S. T.;  
 641 Schmitt, C.: Cirrus optical properties observed with lidar, radiosonde and satellite over the tropical  
 642 indian ocean during the aerosol-polluted northeast and clean maritime southwest monsoon. *J.*  
 643 *Geophys. Res.*, v. 112, p. D17205, 2007.
- 644 Silva, V. B. S., Kousky, V. E., and Higgins, R. W.: Daily Precipitation Statistics for South America: An  
 645 Intercomparison between NCEP Reanalyses and Observations. *J. Hydrometeorol.*, 12, 101-117.  
 646 DOI: 10.1175/2010JHM1303.1, 2011.
- 647 Starr, D. O'C., and Quante, M.: Dynamical processes in cirrus clouds: Concepts and models. Chapter 18  
 648 in: D. Lynch, K. Sassen, D.O'C. Starr, G. Stephens (eds.): *Cirrus*. Oxford University Press, New  
 649 York, 375-396, 2002.
- 650 Stubenrauch, C. J., Chédin, A., Rädcl, G., Scott, N. A., and Serrar, S.: Cloud Properties and Their  
 651 Seasonal and Diurnal Variability from TOVS Path-B. *J. Climate*, 19, 5531–5553, 2006.
- 652 Tanaka, L. M. d. S., Satyamurty, P., and Machado, L. A. T.: Diurnal variation of precipitation in central  
 653 Amazon Basin. *Int. J. Climatol.* 34, 3574–3584, DOI: 10.1002/joc.3929, 2014.



- 654 Thorsen, T. J., Qiang, F., and Comstock, J. M.: Comparison of the CALIPSO satellite and ground-based  
 655 observations of cirrus clouds at the ARM TWP sites, *J. Geophys. Res.*, 116, D21203,  
 656 doi:10.1029/2011JD015970, 2011.
- 657 Wang, T., and Dessler, A. E.: Analysis of cirrus in the tropical tropopause layer from CALIPSO and MLS  
 658 data: A water perspective, *J. Geophys. Res.*, 117, D04211, doi:10.1029/2011JD016442, 2012.
- 659 Wendisch, M., et al.: The ACRIDICON-CHUVA campaign: Studying tropical deep convective clouds  
 660 and precipitation over Amazonia using the new German research aircraft HALO. *Bull. Am. Met.*  
 661 *Soc.*, accepted, doi:10.1175/BAMS-D-14-00255.1, 2016
- 662 Wylie, D. P., Jackson, D. L., Menzel, W. P., and Bates, J. J.: Trends in global cloud cover in two decades  
 663 of HIRS observations. *J. Climate*, 18, 3021–3031, 2005.
- 664 Yang, P., Hong, G., Dessler, A. E., Ou, S. C., Liou, K. N., Minnis, P., and Hashvardhan,: Contrails and  
 665 induced cirrus: Optics and radiation. *Bull. Amer. Meteor. Soc.*, 91, 473–478, 2010a.
- 666 Yang, Q., Fu, Q., and Hu, Y.: Radiative impacts of clouds in the tropical tropopause layer, *J. Geophys.*  
 667 *Res.*, 115, D00H12, doi:10.1029/2009JD012393, 2010b.
- 668 Young, S.: Analysis of lidar backscatter profiles in optically thin cirrus, *Appl. Opt.*, 34, 7019–7031, 1995.
- 669 Zerefos, C. S., Eleftheratos, K., Balis, D. S., Zanis, P., Tselioudis, G., and Meleti, C.: Evidence of impact  
 670 of aviation on cirrus cloud formation, *Atmos. Chem. Phys.*, 3, 1633–1644, doi:10.5194/acp-3-  
 671 1633-2003, 2003.
- 672



Tables:

Table 1. Summary of some recent cirrus clouds studies based on at least a few months of ground-based lidar observations in the tropics and mid-latitudes. The first columns show the period of study and laser wavelength (nm) for each site location, for which more than one study might be available. The cirrus characteristics are those reported by the different authors, which might include: base and top height (km), thickness (km), base and top temperature ( $^{\circ}\text{C}$ ), frequency of occurrence (%) and lidar-ratio (sr).

Measurement site	Location	Period of study	Wave length [nm]	Height [km]			Average values			LR[sr]			
				Base	Top	Thick.	Temp. [°C]	Base	Top			Frequency [%]	SVC
Salt Lake City, Utah, USA	40.8°N 111.8°W	1986 to 1996	694	8.8	11.2	1.8		-34.4	-53.9	50	-		Sassen and Campbel (2001)
Haute Prov., France	43.9°N 5.7°E	1997 to 2007	532/1064	9.3	10.7	1.4				38		18.2	Goldfarb et al. (2001) Hoareau et al. (2013)
Thessaloniki, Greece	40.6°N 22.9°E	2000 to 2006	355/532	8.6	11.7	2.7		-38	-65		57	30	Giannakaki et al. (2007)
Seoul, South Korea	37°N 127°E	2006 to 2009	532/1064	8.8	10.6							20	Kim et al. (2009)
Buenos Aires, Argentina	34.6°S, 58.5°W	2001 to 2005	532	9.6	11.8	2.4		-64.5					Lakkis et al.(2008)
Reunion Island	21°S, 55°E	1996 to 2001	532	11	14					65		18.3	Cadet et al. (2003)
Camagney, Cuba	21.4° N, 77.9° W	1993 to 1998	532	11.6	13.8					25		10	Antuña and Barja, (2006)
Gadanki, India	13.5° N, 79.2° E	1998 to 2013	532	13.0	15.3	2.3		-65	-65	52	36	25	Pandit et al., (2015)
Hulule. Maldives	4.1°N, 73.3°E	1999, 2000	532	11.9	13.7	1.8		-50	-65	15	49	32	Seifert et al. (2007)
Mahe', Seychelles	4.4°S, 55.3°E	Feb-Mar 1999	532			0.2-2.0						19	Pace et al., (2003)
Nauru Island	0.5°S, 166.9°E	Apr-Nov 1999	532	-14	-16								Comstock et al. (2002)



Table 2. Mean cirrus cloud properties and standard deviation in parenthesis for all cirrus clouds, for cirrus clouds above and below 14 km and cirrus clouds with base below and top above 14 km. These cloud properties are also informed to total time of observation, wet, transition and dry seasons

<i>Relative?</i>	<i>All Cirrus Clouds</i>	<b>Total</b>	<b>Wet</b>	<b>Transition</b>	<b>Dry</b>
Frequency of Occurrence [%]		67.2	82.2	79.4	55.5
Base Altitude [km]		12.7 (2.3)	12.7 (2.6)	12.5 (2.4)	12.8 (2.1)
Top Altitude [km]		14.4 (2.0)	14.5 (2.2)	14.3 (2.2)	14.4 (1.8)
Thickness [km]		1.7 (1.5)	1.9 (1.6)	1.8 (1.4)	1.6 (1.4)
Cloud Optical Depth		0.36 (1.20)	0.46 (1.49)	0.38 (1.22)	0.27 (0.90)
Max Backscatter Altitude [km]		13.2 (2.3)	13.2 (2.5)	13.0 (2.4)	13.3 (2.0)
Temperature Max. Back. Alt. [°C]		-58.1 (16.9)	-58.0 (18.2)	-56.3 (18.6)	-59.1 (14.8)
Lidar Ratio [sr]		20.2 (7.0)	18.5 (6.5)	19.4 (6.3)	21.3 (7.2)
Subvisual Cirrus [%]		40.0	36.4	33.9	46.0
Thin Cirrus [%]		37.7	37.0	41.7	36.2
Opaque Cirrus [%]		22.3	26.6	24.4	17.7
<b><i>Cirrus Clouds with Base &gt; 14 km</i></b>					
Fraction of all cirrus [%]		31.8	32.0	28.7	33.2
Base Altitude [km]		15.4 (1.0)	15.7 (1.1)	15.5 (1.0)	15.2 (0.8)
Top Altitude [km]		16.2 (0.9)	16.6 (0.9)	16.4 (0.9)	15.9 (0.8)
Thickness [km]		0.8 (0.6)	1.0 (0.8)	1.0 (0.7)	0.7 (0.4)
Cloud Optical Depth		0.03 (0.06)	0.04 (0.07)	0.04 (0.07)	0.02 (0.04)
Lidar Ratio [sr]		22.9 (9.5)	20.2 (8.7)	21.7 (9.0)	25.5 (9.7)
<b><i>Cirrus Clouds with Top &lt; 14km</i></b>					
Fraction of all cirrus [%]		38.0	38.8	41.9	35.3
Base Altitude [km]		10.8 (1.5)	10.7 (1.5)	10.5 (1.5)	11.2 (1.3)
Top Altitude [km]		12.3 (1.4)	12.3 (1.4)	12.1 (1.3)	12.5 (1.3)
Thickness [km]		1.5 (1.2)	1.6 (1.2)	1.6 (1.2)	1.3 (1.0)
Cloud Optical Depth		0.50 (1.70)	0.67 (2.09)	0.55 (1.64)	0.32 (1.28)
Lidar Ratio [sr]		20.0 (6.7)	19.3 (7.7)	18.9 (6.2)	20.5 (6.4)
<b><i>Cirrus Clouds with Base &lt; 14km and Top &gt; 14 km</i></b>					
Fraction of all cirrus [%]		30.2	29.2	29.3	31.5
Base Altitude [km]		12.2 (1.4)	11.2 (1.5)	12.3 (1.3)	12.3 (1.3)
Top Altitude [km]		15.2 (0.9)	15.3 (1.0)	15.3 (0.9)	15.0 (0.7)
Thickness [km]		3.0 (1.7)	3.3 (1.9)	2.9 (1.5)	2.8 (1.5)
Cloud Optical Depth		0.55 (0.99)	0.70 (1.19)	0.49 (1.01)	0.47 (0.78)
Lidar Ratio [sr]		19.7 (6.3)	18.0 (5.5)	19.1 (5.6)	20.9 (6.7)



Figures:



Figure 1. Location of the experimental site ( $2.89^{\circ}\text{S}$   $59.97^{\circ}\text{W}$ ) is shown, 30 km upwind from downtown Manaus-AM, Brazil.

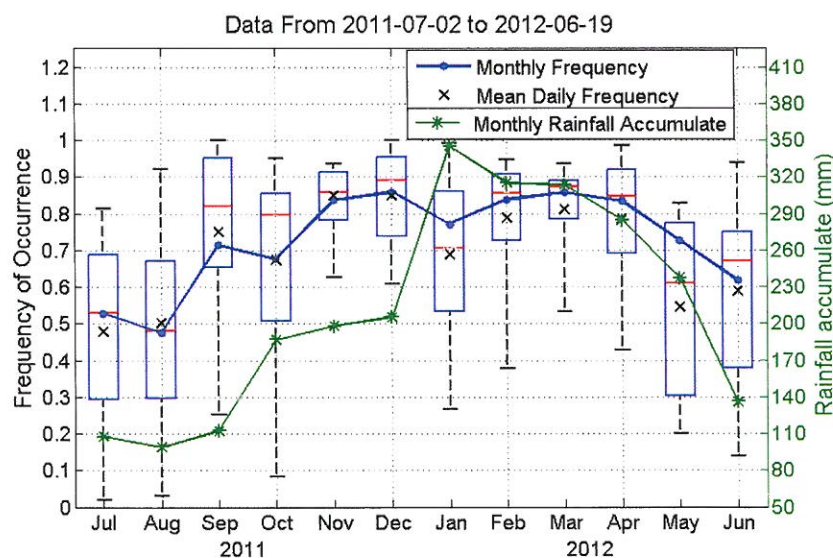


Figure 2. Monthly frequency of occurrence of cirrus clouds from July 2011 to June 2012 (blue line). Red dashes (black x) in the boxplots are the median (mean) of the daily frequency in each month. The edges of the boxes are the 25th and 75th percentiles, and the whiskers extend to the most extreme daily values. Accumulated rainfall is shown in green on the right axis. Data is from TRMM 3B42 version 7.

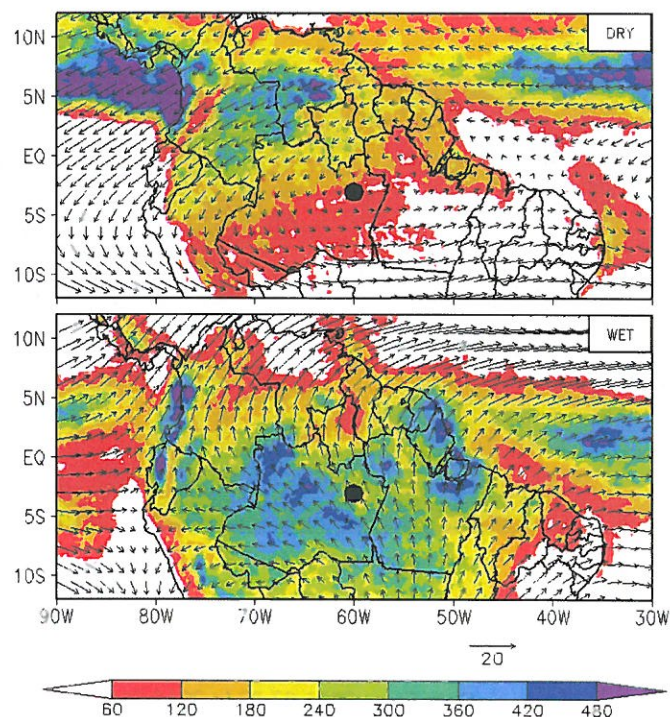


Figure 3. Mean precipitation (colors, mm/day) from the TRMM 3B42 version 7 and mean wind field (vectors, m/s) at 200 hPa from ECMWF ERA Interim reanalysis are shown for the average dry months (JJAS) and wet months (JFMA), between July 2011 and June/2012. The experimental site location is marked with a black dot.

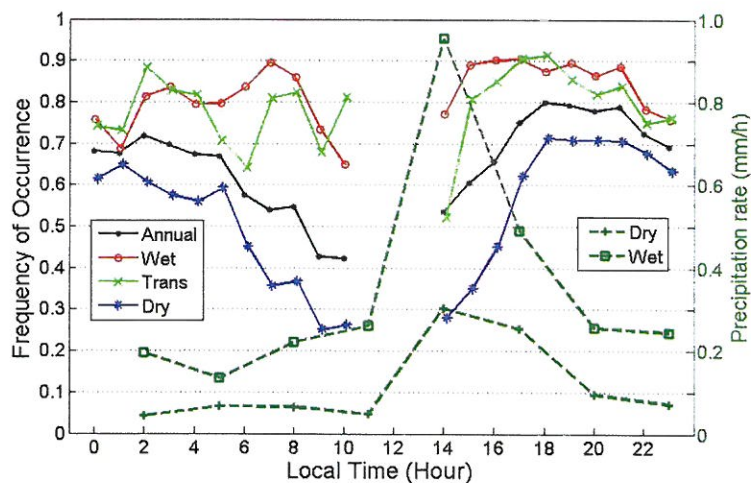


Figure 4. Diel cycles of the hourly frequency of occurrence of cirrus clouds are shown for the annual, wet, transition and dry periods. Mean precipitation rate (mm/h) over an area of  $2^\circ \times 2^\circ$  centered in the site is shown in dashed lines for the Dry (+) and wet (□) periods. Data is from TRMM version 7.

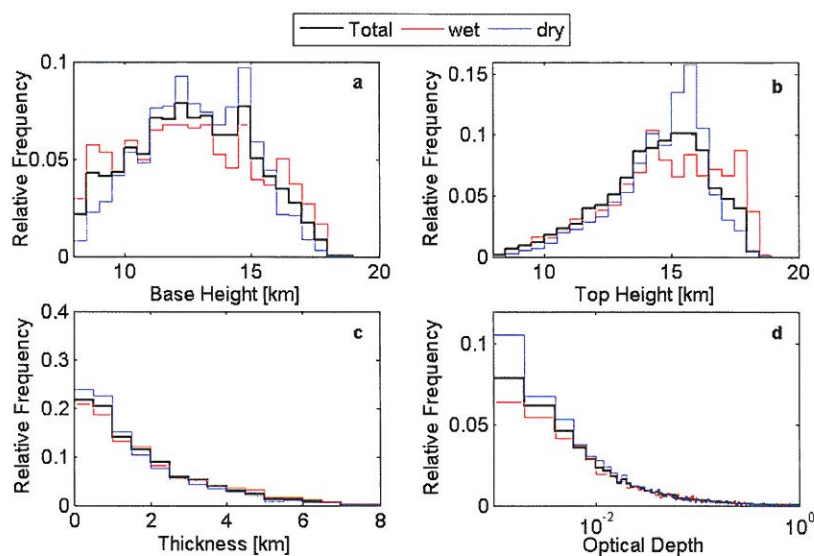


Figure 5. Panels show the normalized histograms of (a) cirrus cloud base, (b) top, (c) geometrical thickness, and (d) optical depth, for the overall period (black), wet season (JFMA, red) and dry season (JJAS, blue).

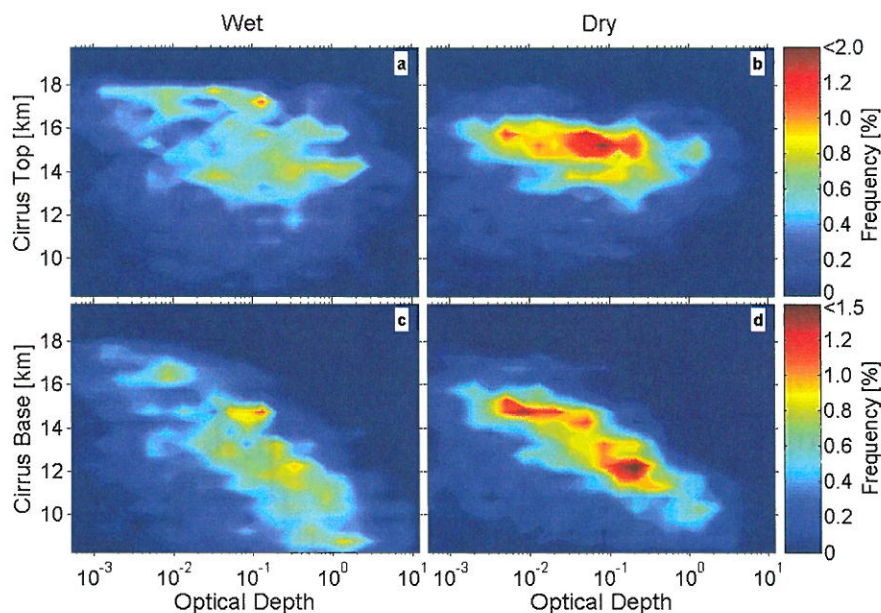


Figure 6. Two-dimensional histograms of cirrus cloud top (top) and cloud base (bottom) with optical depth during the wet (left) and dry (right) months are shown.

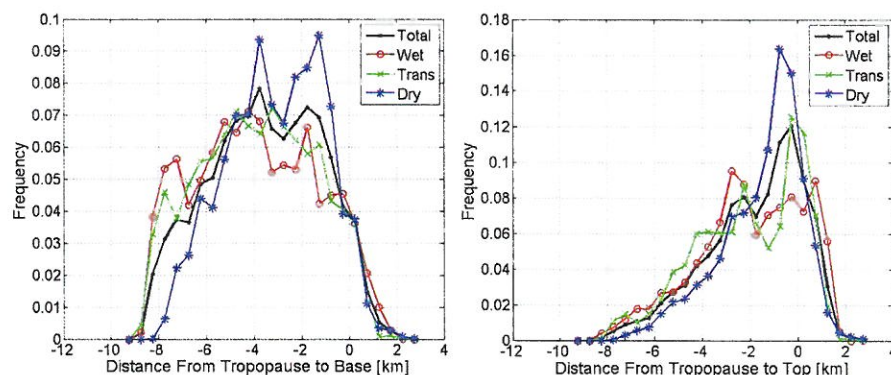


Figure 7. Normalized histograms of the distance of the tropopause to the cirrus base (left) and top (right) are shown for overall period (black) and each season (colors). Negative values mean that clouds are below tropopause. The average tropopause altitude was  $16.2 \pm 0.4$  km.

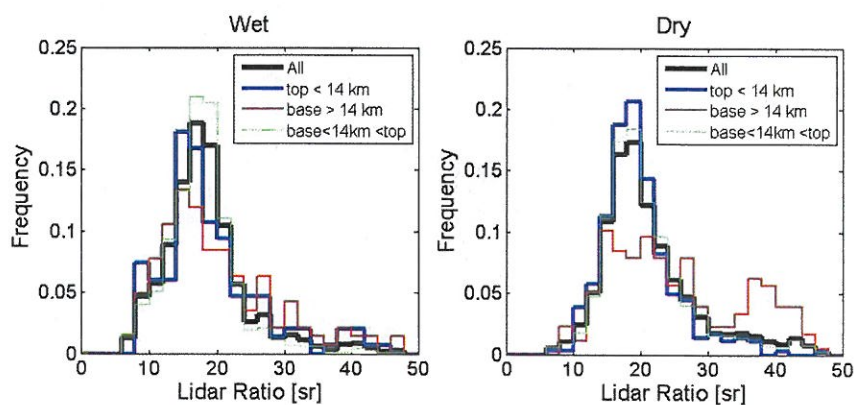


Figure 8. Normalized histograms of the lidar ratio for the wet (left) and dry (right) months are shown for all clouds (black) and clouds with base above 14 km (red), top below 14 km (blue) and cloud with top (base) above (below) 14 km (green).

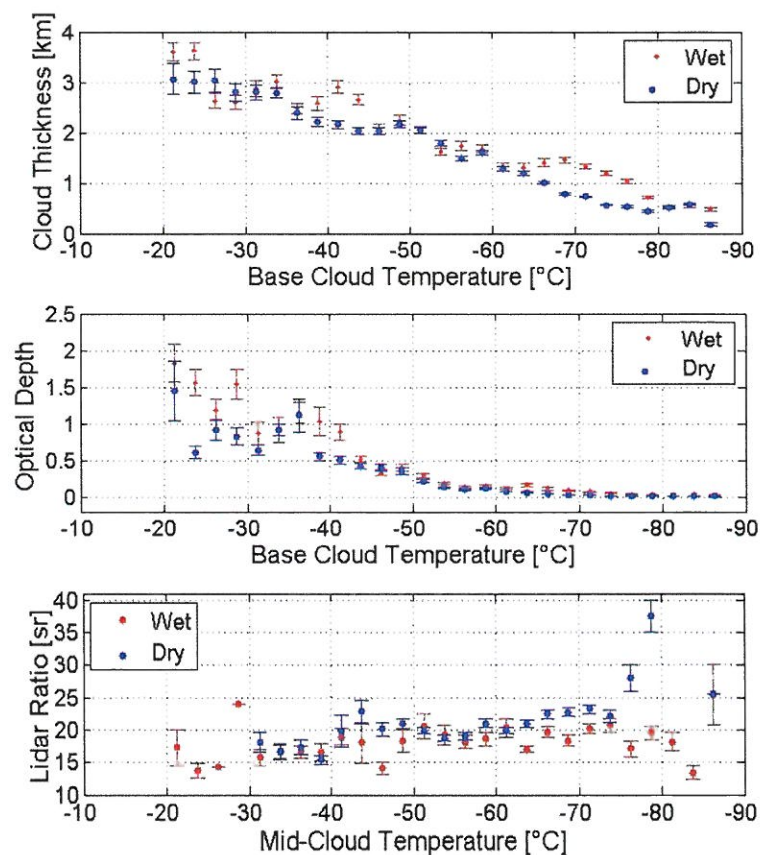


Figure 9. Dependence of the geometrical thickness, cloud optical depth and lidar ratio with temperature. Temperature are shown in 2.5 °C intervals and the other variables with their mean and standard deviation in each temperature interval.

